

## ORIGINAL ARTICLE

# Calculation of the Choroidal Vascularity Index and Tissue Distribution Indexes in Different Retinal and Choroidal Regions by Employing Digital Image Processing Techniques in Optical Coherence Tomography Images

## Optik Koherens Tomografi Görüntülerinde Dijital Görüntü İşleme Teknikleri Kullanılarak Farklı Retina ve Koroid Bölgelerindeki Koroid Vaskülarite İndeksi ve Doku Dağılım İndekslerinin Hesaplanması

<sup>1,2</sup>Onur Inam , <sup>3</sup>Deniz Somer , <sup>3</sup>Güner Özkan Üney , <sup>4</sup>Abdullah Ruhi Soylu 

<sup>1</sup>Department of Biophysics, Faculty of Medicine, Gazi University, Ankara, Türkiye

<sup>2</sup>Department of Ophthalmology, Edward S. Harkness Eye Institute, Vagelos College of Physicians and Surgeons, Columbia University Irving Medical Center, New York, NY, USA

<sup>3</sup>Clinic of Ophthalmology, Ankara Training and Research Hospital, University of Health Sciences, Ankara, Türkiye

<sup>4</sup>Department of Biophysics, Faculty of Medicine, Hacettepe University, Ankara, Türkiye

## Correspondence

Onur Inam, Department of Biophysics, Faculty of Medicine, Gazi University, Ankara, Türkiye / Department of Ophthalmology, Edward S. Harkness Eye Institute, Vagelos College of Physicians and Surgeons, Columbia University Irving Medical Center, New York, NY, USA

E-Mail: [onurinam@gazi.edu.tr](mailto:onurinam@gazi.edu.tr)

## How to cite ?

Inam O, Somer D, Üney G, Soylu A. Calculation of the Choroidal Vascularity Index and Tissue Distribution Indexes in Different Retinal and Choroidal Regions by Employing Digital Image Processing Techniques in Optical Coherence Tomography Images. Genel Tıp Derg. 2023;33(6):785-95.

## ABSTRACT

**Objective:** In this study, it was aimed to investigate the optical coherence tomography (OCT) images of healthy subjects for various parameters and tissue distribution indexes.

**Materials and Methods:** One hundred eyes of 50 healthy subject's OCT images have been employed for analysis. Total retinal area (TRA), dark retinal area (DRA), light retinal area (LRA), dark area percent (DAP) and light area percent (LAP) as retinal measurements; total choroidal area (TCA), luminal choroidal area (LCA), stromal choroidal area (SCA), luminal area percent or choroidal vascularity index (CVI) and stromal area percent (SAP) as choroidal measurements have been investigated for vertical and horizontal OCT scans. 6500 µm of the total retinal and choroidal area have been binarized and analyzed in 100 µm intervals and further divided into three main parts: inner, middle and outer.

**Results:** CVI value for the entire vertical scan is 69.2±2.6, whereas the entire horizontal scan is 70.1±2.7 (p=0.019). Entire inner part CVI of the vertical scans are calculated as 74.5±4.6 and in horizontal scans as 74.8±5.0 (p=0.678). Vertical CVI of the entire middle part has higher values with 67.2 ± 3.9 than the horizontal scans with 66.0±4.1 (p=0.025). This was conversely recorded in the entire outer part, the vertical CVI value of which is 66.6±4.3 and horizontal CVI value is 70.3±4.7 (p<0.001). Although there was no statistically significant difference between vertical and horizontal scans for entire region, inner, middle and outer regions in any of the TRA comparisons (p=0.386, p=0.422, p=0.309 and p=0.352 respectively), vertical TCA measurements were significantly higher than the horizontal scans (p=0.010, p=0.013, p=0.012 and p=0.008, respectively).

**Conclusion:** CVI and other parameters and tissue distribution indexes could be a valuable tool for differentiating and evaluating the retinal and choroidal conditions in different scan regions.

**Keywords:** Biophysics, Image Processing, Optical Coherence Tomography, Retina, Choroid

## ÖZ

**Amaç:** Bu çalışmada, sağlıklı bireylerin optik koherens tomografi görüntülerinin çeşitli parametreler ve doku dağılım indeksleri açısından incelenmesi amaçlanmaktadır.

**Gereç ve Yöntemler:** Elli sağlıklı bireyin 100 gözünün optik koherens tomografi (OKT) görüntüleri analiz için kullanılmıştır. Toplam retina alanı (TRA), karanlık retina alanı (DRA), aydınlık retina alanı (LRA), karanlık alan yüzdesi (DAP) ve aydınlık alan yüzdesi (LAP) gibi retina ölçümleri; toplam koroid alanı (TCA), lüminal koroid alanı (LCA), stromal koroid alanı (SCA), lüminal alan yüzdesi veya koroid vaskülarite indeksi (CVI) ve stromal alan yüzdesi (SAP) gibi koroid ölçümleri, dikey ve yatay OKT taramaları için incelendi. Toplam retinal ve koroid alanının 6500 µm'si 100 µm aralıklarla binarize hale getirilip analiz edildi ve daha sonra iç, orta ve dış olmak üzere üç ana bölüme ayrıldı.

**Bulgular:** Tüm dikey tarama CVI değeri 69,2±2,6 iken, tüm yatay tarama için bu değer 70,1±2,7 olarak hesaplandı (p=0,019). Dikey taramalar için tüm iç bölüm CVI değeri 74,5±4,6 ve yatay taramalar için 74,8±5,0 olarak hesaplandı (p=0,678). Tüm orta bölüm dikey CVI değeri 67,2 ± 3,9 iken yatay taramalarda 66,0±4,1 olarak bulundu (p=0,025). Bu durum tüm dış bölüm için tersiydi; dikey CVI değeri 66,6±4,3 iken yatay CVI değeri 70,3±4,7 olarak bulundu (p<0,001). TRA karşılaştırmalarının hiçbirinde, tüm bölüm, iç bölüm, orta bölüm ve dış bölüm için dikey ve yatay taramalar arasında istatistiksel olarak anlamlı fark bulunmadı (sırasıyla p=0,386, p=0,422, p=0,309 ve p=0,352). Ancak dikey TCA ölçümleri, yatay taramalara göre istatistiksel olarak anlamlı şekilde yüksek bulundu (sırasıyla p=0,010, p=0,013, p=0,012 ve p=0,008).

**Sonuç:** CVI, diğer parametreler ve doku dağılım indeksleri, farklı tarama bölgelerinde retinal ve koroid durumları ayırt etmek ve değerlendirmek için değerli bir araç olabilir.

**Anahtar Kelimeler:** Biyofizik, Görüntü İşleme, Optik Koherens Tomografi, Retina, Koroid

## Introduction

The retina, a delicate and complex neurosensory tissue located in the inner layer of the eye, is responsible for converting incoming light stimuli into electrical signals that can be processed and interpreted by the visual system (1, 2). Retinal thickness is not constant and

exhibits significant variation across different topographic locations within the eyeball (1, 3). Choroid is a specialized vascular tissue that supplies mainly the outer retina (4). Choroid is not only a tissue that supplies blood but has other functions like regulating heat, the position of the

retina, and secretion of growth factors (4). As a part of the uveal tissue, choroid is located in the middle layer of the eyeball, between retinal and scleral layers (4, 5). It has some other critical biophysical functions in the regulation of intraocular pressure (IOP), regulation of the emmetropization which is mainly an optical issue, uveoscleral aqueous humor drainage which accounts for approximately 35% of total drainage (4, 6, 7). Choroid is composed of different layers such as Bruch Membrane, choriocapillaris, Haller's layer (HL), Sattler's layer (SL) and suprachoroidea, respectively (4, 5).

While the functional importance of the retina and choroid for the basic sciences like biophysics, physiology, and histology is improving, an exceptional tool called optical coherence tomography (OCT) has emerged, changing the imaging quality of these structures close to histological quality (8, 9). This technique is noninvasive and time-saving, which makes it an essential part of the ophthalmological examination nowadays (8-10). First described in 1991, it uses low coherence interferometry which is basically similar to the ultrasonic pulse-echo equivalent but the difference is that it uses near-infrared light beams (NIR), instead of sound waves, and this initially designed OCT is called time domain OCT (TD-OCT) (11). Eyeball, as a clear optical system offer to the OCT a suitable environment, thus, it has become popular in ophthalmology in years, images obtained via OCT has reshaped the imaging and management of diseases (12-16). After the first OCT designs, spectral domain OCT (SD-OCT) or Fourier domain OCT has emerged (17). SD-OCT detects light as a total of functions of wavelength, which gives a speed advantage of 50-100 times compared to its previous ancestor TD-OCT (9, 17). This advantage turns into a massive increase at the axial resolution up to 2  $\mu\text{m}$  and 100,000 A-scans per second (18, 19). Even better images for the choroidal region has been obtained using enhanced depth imaging (EDI-OCT) technique, in which the scanner is closer to the choroid in order to obtain an inverted and deeper layer of images, which in turn visualize choroidal layers better (20).

While OCT is a valuable biomedical imaging tool, biophysical image processing techniques have been proven to improve the value of the outcome further (21). Various image processing techniques, particularly in the choroidal region, has been investigated for both in healthy eyes and diseased ones and this index and parameters have been proven to be a valuable option to differentiate, diagnose and follow up diseases (21-26). Considering the distinct layer variations present in both retinal and choroidal tissues, which are observable in OCT images but have not been quantified and characterized in detail, this study aims to identify differences that may arise within OCT images across various regions of the retina and choroid using biophysical image processing techniques.

## Materials and Methods

### Research Location, Time and Sampling

This retrospective cross-sectional study was conducted at the Department of Biophysics, Faculty of Medicine,

Hacettepe University. A total of 100 eyes from 50 subjects (25 Female, 25 Male) were included. All of the subject's images and information have been obtained from the Clinic of Ophthalmology, Ankara Training and Research Hospital, University of Health Sciences.

### Inclusion Criteria

Subjects admitted to the Clinic of Ophthalmology, Ankara Training and Research Hospital, University of Health Sciences within the last three years before August 2017, and who were between 15-65 years old, had no prior known ocular disease history, had no prior known systemic disease history, had no prior known ocular surgery history, had conventional and computer-based archive data that could be reachable, had SD-OCT and EDI-OCT images in Spectralis (Heidelberg Engineering, Heidelberg, Germany), had vertical and horizontal images, had SD-OCT images with enough quality for interpretation were included in the study.

### Data Collection Tool

Both conventional hospital archives and computer-based archives were utilized as data collection tools in addition to the data obtained from the SD-OCT device. Information such as age, gender, demographic details, ocular disease history, systemic disease history, and history of ocular surgeries were retrospectively gathered and documented. All the obtained data were recorded within the computerized database. SD-OCT images were extracted using the device's own program.

### Data Collection Process

Subjects who fulfilled the inclusion criteria were enrolled as study subjects. From this pool, 25 female and 25 male subjects were randomly selected, resulting in a total of 50 subjects, 100 eyes, 200 images consisting of 100 horizontal scans and 100 vertical scans.

### Gathering the Image

Images of the randomly selected patients were collected using the SD-OCT device and exported using the export function within the device's main program. Images were saved in the joint photographic expert's group (JPEG) file format and included a scale for reference. The default image frame size was 1264 x 596 pixels, featuring a fundus infrared (IR) image on the left side and an OCT image on the right side. The OCT scale was not uniform in both height and width; it was expanded vertically to enhance visualization. All measurements were conducted in accordance with the scale's axes.

### Image Processing at Fiji/ImageJ

Following the export process, the images were opened using the Fiji/ImageJ program (version 1.52d) (27, 28). The Fiji/ImageJ program serves as an open-source image processing software that can be easily obtained from the internet. Researchers have the capability to create codes tailored to their specific projects, thereby enhancing the utility of Fiji/ImageJ. The Fiji program is essentially an advanced version of ImageJ, featuring several useful pre-downloaded

plug-ins. For our study, we found it more convenient to utilize the Fiji program.

### Setting Scale

To conduct measurements in actual dimensions, it is essential to accurately set the scales for consecutive images. Upon measuring the desired distance, the researcher can proceed by selecting the "set scale" button found under the "analyze" tab. This action allows for the adjustment of the scale to its real-world length. Upon confirming the new scale, subsequent measurements will be carried out by the program based on the original scale.

### Retinal And Choroidal Region of Interest Drawing

Region of Interest (ROI) were drawn based on the horizontal scale. Specifically, a 6500  $\mu\text{m}$  area centered around the fovea was drawn for the retina. In the retinal ROI, the inner border was defined as the boundary between the internal limiting membrane (ILM) and the vitreoretinal margin, while the outer border was determined by the hyperreflective outer margin of the retinal pigment epithelium (RPE) layer. For the choroidal ROI, the inner border was demarcated by the hyperreflective outer margin of the RPE layer, and the outer border was established at the choroidoscleral junction.

### Sampling Rate

In our study, we discovered that all 200 images exhibited retinal and choroidal boundaries within a range of 6500  $\mu\text{m}$  centered around the fovea. With the aim of extracting standardized data from both horizontal and vertical scans, we opted for a total area of 6500  $\mu\text{m}$  centered on the fovea, equally divided into 3250  $\mu\text{m}$  on each side.

In vertical scans, regions of interest (ROI) were selected as 3250  $\mu\text{m}$  inferior and 3250  $\mu\text{m}$  superior, while in horizontal scans, the chosen ROI consisted of 3250  $\mu\text{m}$  nasal and 3250  $\mu\text{m}$  temporal areas. These defined 6500  $\mu\text{m}$  ROIs were applied to both the retina and the choroid. Each 6500  $\mu\text{m}$  ROI was further subdivided into 65 equal segments, each spanning a width of 100  $\mu\text{m}$ . Each segment was labeled according to its distance in micrometers from the center of the fovea. For instance, "horizontal central-0" represents the area encompassing the central point (0 center) with 50  $\mu\text{m}$  extending nasally and 50  $\mu\text{m}$  extending temporally. "Inferior-1000" corresponds to the region 1000  $\mu\text{m}$  below the center of the fovea, spanning between 950  $\mu\text{m}$  and 1050  $\mu\text{m}$  below the center. Similarly, the final segment on each margin is denoted as "3200  $\mu\text{m}$  inferior," "3200  $\mu\text{m}$  superior," "3200  $\mu\text{m}$  nasal," or "3200  $\mu\text{m}$  temporal." Results designated for inferior regions are abbreviated as I, superior as S, nasal as N, temporal as T, horizontal as H and vertical as V. The remaining number part in the tables addresses the distance from 0 to 3200  $\mu\text{m}$ .

### Processed Areas

The total vertical area and all vertically processed 65 area have been further horizontally divided into

three portions as inner, middle and outer portions. These areas were divided equally into three, based on their original heights. Consequently, the entire total area was separated into three sections, and the 65 smaller vertical segments were further divided into a total of 195 sub-segments. This additional level of division was implemented to enhance the precision of quantification and facilitate a more thorough analysis of various sections within the retina and choroid.

### Binarizing Process

To perform the binarization process, the image type was set to a "8-bit" grayscale. To achieve this, under the "image" tab, the "type" option, then "8-bit." was chosen. Next, under the "image" tab, "adjust" option was clicked and "auto local threshold" was selected. Within this section, "Niblack" method was chosen as previously mentioned (21). By executing this command, the binarized image was obtained as the resulting output.

### Analyzed Parameters

Total retinal area (TRA), dark retinal area (DRA), light retinal area (LRA), dark area percent (DAP), light area percent (LAP), total choroidal area (TCA), luminal choroidal area (LCA), stromal choroidal area (SCA), luminal area percent or choroidal vascularity index (CVI), and stromal area percent (SAP) parameters were analyzed for entire retinal and choroidal ROIs and also 65 regions with an interval of 100  $\mu\text{m}$ , and further investigated for inner, middle and outer layers for each of the entire and smaller ROIs.

These parameters and indexes were measured through a semi-automated way using codes generated within the Fiji/ImageJ program (29).

### Statistical Analysis

The data collected in this study were stored in a computer file. These files were imported into SPSS for statistical analysis using SPSS 21.0 (IBM SPSS Statistics V21.0). The presentation of graphical demonstrations was carried out using both SPSS 21.0 and Microsoft Excel (Microsoft Excel for Mac V16.11) programs. Descriptive statistics were utilized for summarizing the data. Qualitative variables were presented using numbers and percentages, while quantitative variables were summarized using the mean, standard deviation, minimum, and maximum values. Normality of the corresponding variables was assessed using the Shapiro-Wilk normality test. For those variables found to be normally distributed, Student's t-test was employed. Conversely, for variables that did not exhibit normal distribution, the Mann-Whitney U test was utilized. A p-value lower than 0.05 was considered statistically significant for all aspects of the study.

### Ethical Committee Approval

This study has received approval from the Hacettepe University Medical Faculty Non-Invasive Clinical Research Ethics Committee, as indicated by the decision dated 11.07.2017 and numbered GO 17-670 and conducted as a doctoral thesis study.

No external resources were sought for the implementation of this study, and no financial or other forms of support were received. Furthermore, there are no conflicts of interest associated with this study.

**Results**

**General Overview and Demographics**

A total of 50 participants (25 females and 25 males) were included in this study. The study involved the examination of both right and left eyes, encompassing horizontal and vertical scans, resulting in the analysis of a total of 200 OCT images. (Table 1.)

The average age at the time of examination was  $40.28 \pm 14.52$  years, ranging from 16 to 62. The mean age for females was  $40.71 \pm 15.08$  years with an age range of 17 to 61. For males, the mean age was  $39.86 \pm 14.24$  years, spanning from 16 to 62. The difference in age between females and males was not statistically significant ( $p=0.838$ ).

**TRA**

TRA measurements were performed on both vertical and horizontal scans involving a total of 100 eyes. In vertical scans, when examining the total regions, the lowest TRA value was recorded at V 0 with a mean value of  $22379.4 \pm 2365.2 \mu\text{m}^2$  while the highest TRA value was observed at S 1200 with a mean value of  $36095.1 \pm 1844.9 \mu\text{m}^2$ . When examining the inner regions of vertical scans, the lowest TRA value occurred at S 200, amounting to  $7029.9 \pm 864.3 \mu\text{m}^2$ , and the highest TRA value within inner regions was registered at S 1200, at  $11808.8 \pm 647.5 \mu\text{m}^2$ . Similarly, for the middle regions of vertical scans, the lowest TRA value was noted at V 0, measuring  $7572.5 \pm 894.8 \mu\text{m}^2$  while the highest TRA value within middle regions was recorded at S 1200 with an average of  $12180.4 \pm 610.1 \mu\text{m}^2$ . As for the outer regions of vertical scans, the lowest TRA value was documented at V 0 with a mean of  $7434.8 \pm 981.7 \mu\text{m}^2$ , while the highest TRA value within outer regions was found at S 1100 averaging  $12019.1 \pm 628.5 \mu\text{m}^2$ . (Figure 1.)

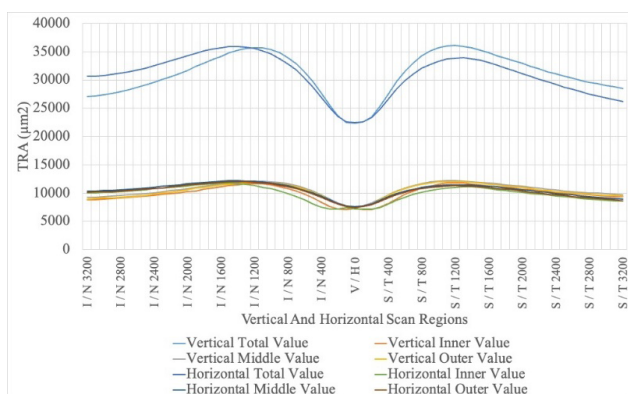


Figure 1. TRA Measurements in Vertical and Horizontal Scan Regions. TRA: Total Retinal Area, I: Inferior, S: Superior, N: Nasal, T: Temporal, H: Horizontal, V: Vertical.

In the context of horizontal scans, when examining the total regions, the lowest TRA value was observed at H 0, registering a mean value of  $22501.5 \pm 2198.2 \mu\text{m}^2$  while the highest TRA value was found at N 1400 with an

average of  $35958.8 \pm 1777.7 \mu\text{m}^2$ . For the inner regions of horizontal scans, the lowest TRA value occurred at N 200, amounting to  $7129.4 \pm 757.2 \mu\text{m}^2$  while the highest TRA value within inner regions was recorded at N 1600 with an average of  $11741.2 \pm 650.6 \mu\text{m}^2$ . Similarly, within the middle regions of horizontal scans, the lowest TRA value was noted at H 0, measuring  $7580.4 \pm 772.4 \mu\text{m}^2$  while the highest TRA value within middle regions was found at N 1400 with a mean of  $12176.5 \pm 593.5 \mu\text{m}^2$ . Concerning the outer regions of horizontal scans, the lowest TRA value was documented at H 0, amounting to  $7435.8 \pm 744.4 \mu\text{m}^2$  while the highest TRA value within outer regions was found at N 1400 averaging  $11970.1 \pm 606 \mu\text{m}^2$ . (Figure 1.)

When we investigate the difference between vertical and horizontal TRA results, there were no statistically significant difference between entire ROI, entire inner part, entire middle part and entire outer part ( $p = 0.386$ ,  $p = 0.422$ ,  $p = 0.309$  and  $p = 0.352$  respectively.). (Table 2.)

**DRA**

Assessments were carried out for DRA on both vertical and horizontal scan orientations, encompassing 100 eyes. Analysis of the total regions in vertical scans revealed the lowest DRA value at V 0 with an average of  $13731.4 \pm 1688.9 \mu\text{m}^2$ , and the highest DRA value was observed at S 1100 with a mean value of  $19997.5 \pm 1579.6 \mu\text{m}^2$ . The inner regions of vertical scans exhibited the lowest DRA value at S 400 amounting to  $2202.9 \pm 839.4 \mu\text{m}^2$ , while the highest DRA value within the inner regions was registered at I 1200 with an average of  $5789.2 \pm 931.6 \mu\text{m}^2$ . Furthermore, the middle regions of vertical scans showed the lowest DRA value at V 0 measuring  $6128.4 \pm 947.1 \mu\text{m}^2$ , and the highest DRA value within middle regions was observed at I 300 with a mean of  $8106.9 \pm 818 \mu\text{m}^2$ . The outer regions of vertical scans documented the lowest DRA value at S 100 with an average of  $2941.2 \pm 852.7 \mu\text{m}^2$ , and the highest DRA value within outer regions was identified at S 1100 averaging  $6780.4 \pm 794.3 \mu\text{m}^2$ .

In the examination of total regions in horizontal scans, it was observed that the lowest DRA value was recorded at T 3200 with a mean value of  $12789.7 \pm 1967.4 \mu\text{m}^2$  whereas the highest DRA value was identified at N 1400 with an average of  $19977.5 \pm 1566.1 \mu\text{m}^2$ . With respect to the inner regions of horizontal scans, the lowest DRA value was documented at T 400, amounting to  $1915.7 \pm 792.7 \mu\text{m}^2$  while the highest DRA value within inner regions was noted at N 1600 with an average of  $5897.1 \pm 754.5 \mu\text{m}^2$ . Correspondingly, within the middle regions of horizontal scans, the lowest DRA value was observed at N 2900, measuring  $5997.5 \pm 829.2 \mu\text{m}^2$  while the highest DRA value within middle regions was recorded at N 1100 with a mean of  $8095.6 \pm 1010.2 \mu\text{m}^2$ . In relation to the outer regions of horizontal scans, the lowest DRA value was documented at T 100 with an average of  $2772.5 \pm 780.2 \mu\text{m}^2$  whereas the highest DRA value within outer regions was identified at N 1300, averaging  $6483.3 \pm 831.9 \mu\text{m}^2$ .

When we further compare the entire DRA measurements of vertical and horizontal scans, we

found a significant difference between entire ROI, entire inner part, and entire outer part although entire middle part was not significantly different ( $p = 0.008$ ,  $p = 0.021$ ,  $p < 0.001$  and  $p = 0.430$  respectively.). (Table 2.)

### LRA

Measurements of LRA were conducted for both vertical and horizontal scans across a sample of 100 eyes. Upon examining the total regions in vertical scans, the recorded LRA value at I 100 was the lowest measuring an average of  $8467.2 \pm 1408.5 \mu\text{m}^2$ , whereas the highest LRA value was observed at I 1300 with a mean value of  $16333.3 \pm 1327.5 \mu\text{m}^2$ . Analysis of the inner regions of vertical scans revealed that the lowest LRA value was documented at I 200, amounting to  $2752 \pm 1105.9 \mu\text{m}^2$ , and the highest LRA value within inner regions was registered at S 700 with an average of  $6624 \pm 827.6 \mu\text{m}^2$ . Similarly, within the middle regions of vertical scans, the lowest LRA value was noted at S 200 measuring  $705.9 \pm 704 \mu\text{m}^2$ , while the highest LRA value within middle regions was found at I 1400 with a mean of  $5172.5 \pm 1021.7 \mu\text{m}^2$ . Furthermore, the outer regions of vertical scans documented the lowest LRA value at V 0 with an average of  $4302.5 \pm 569.7 \mu\text{m}^2$  while the highest LRA value within outer regions was identified at I 500, averaging  $5305.4 \pm 539.3 \mu\text{m}^2$ .

In the examination of total regions in horizontal scans, the LRA value was observed to be at its lowest at N 100 with a mean value of  $8471.1 \pm 1687.6 \mu\text{m}^2$  whereas the highest LRA value was detected at N 1600 with an average of  $16225 \pm 1280.2 \mu\text{m}^2$ . In the inner regions of horizontal scans, the lowest LRA value was observed at N 200, measuring  $2685.8 \pm 1086.5 \mu\text{m}^2$  while the highest LRA value within the same regions was recorded at N 700 with an average of  $6430.9 \pm 651.6 \mu\text{m}^2$ . Similarly, within the middle regions of horizontal scans, the lowest LRA value was noted at T 200 with a measurement of  $700.0 \pm 788.5 \mu\text{m}^2$  while the highest LRA value within middle regions was found at N 1700 with a mean of  $4925 \pm 913.1 \mu\text{m}^2$ . With regard to the outer regions of horizontal scans, the lowest LRA value was documented at H 0 with an average of  $4504.4 \pm 562.7 \mu\text{m}^2$  while the highest LRA value within the same regions was identified at T 2100, averaging  $5639.2 \pm 525.7 \mu\text{m}^2$ .

Comparing the entire LRA measurements in vertical and horizontal scans, the difference is significantly prominent in the entire ROI, middle and outer parts, but not in the inner parts ( $p = 0.013$ ,  $p = 0.033$ ,  $p < 0.001$  and  $p = 0.238$  respectively.). (Table 2.)

### DAP

Measurements of DAP were conducted on 100 eyes, using both vertical and horizontal scans. The lowest DAP value was recorded at S 500 during vertical scans with a mean value of  $50.3 \pm 4.1\%$ , while the highest DAP value was observed at I 100 with an average of  $62.4 \pm 4.2\%$  when examining the total regions. For the inner regions of vertical scans, the lowest DAP value was registered at S 400, amounting to  $26.5 \pm 7.8\%$  while

the highest DAP value within inner regions was noted at I 200 with an average of  $61.7 \pm 12\%$ . Analogously, within the middle regions of vertical scans, the lowest DAP value was reported at I 1400, measuring  $56.6 \pm 8.1\%$ , and the highest DAP value within middle regions was found at S 200 with a mean of  $91.9 \pm 7.2\%$ . In terms of the outer regions of vertical scans, the lowest DAP value was documented at I 100 with an average of  $38.2 \pm 8.5\%$  while the highest DAP value within outer regions was identified at I 1200, averaging  $56.9 \pm 5.6\%$ .

In the context of horizontal scans, a discernible pattern emerged regarding the distribution of DAP values among various regions. Specifically, upon examining the total regions, it was observed that the lowest DAP value was determined at T 3200, exhibiting a mean value of  $48.6 \pm 5.5\%$ . Conversely, the highest DAP value was recorded at N 100 with an average of  $62.7 \pm 4.9\%$ . Turning to the inner regions of horizontal scans, it was found that the lowest DAP value occurred at T 400, amounting to  $23.6 \pm 8.5\%$ . Moreover, the highest DAP value within inner regions was noted at N 200 with an average of  $62.8 \pm 11.9\%$ . Similarly, the middle regions of horizontal scans exhibited a comparable pattern: the lowest DAP value was seen at N 2600, measuring  $57 \pm 8.2\%$ , and the highest DAP value within middle regions was found at T 200 with a mean of  $91.7 \pm 8.8\%$ . Finally, with respect to the outer regions of horizontal scans, the lowest DAP value was documented at T 3200 with an average of  $35.4 \pm 7.4\%$ , while the highest DAP value within outer regions was identified at N 1700, averaging  $54.3 \pm 5.8\%$ .

Combining and comparing the vertical and horizontal results, entire ROI DAP measurements were found significantly higher in the vertical scans compared to the horizontal scans ( $p < 0.001$ ). This difference in vertical DAP measurements for all entire inner, middle and outer parts were statistically higher compared to the horizontal analogues ( $p = 0.003$ ,  $p = 0.048$  and  $p < 0.001$ , respectively.). (Table 2.)

### LAP

LAP was employed to measure both vertical and horizontal scans across a sample of 100 eyes. In vertical scans, the lowest LAP value was observed at I 100 when examining the total regions with a mean value of  $37.6 \pm 4.2\%$ . Conversely, the highest LAP value was found at S 500 with an average of  $49.7 \pm 4.1\%$ . Within the inner regions of vertical scans, the lowest LAP value occurred at I 200, amounting to  $38.3 \pm 12\%$  while the highest LAP value within this area was recorded at S 400 with an average of  $73.5 \pm 7.8\%$ . Similarly, within the middle regions of vertical scans, the lowest LAP value was noted at S 200 measuring  $8.1 \pm 7.2\%$  while the highest LAP value within this region was found at I 1400 with a mean of  $43.4 \pm 8.1\%$ . Regarding the outer regions of vertical scans, the lowest LAP value was documented at I 1200 with an average of  $43.1 \pm 5.6\%$  while the highest LAP value within these regions was identified at I 100, averaging  $61.8 \pm 8.5\%$ .

In the study of horizontal scans, the regions were examined and it was observed that the LAP value

was at its lowest point at N 100 with a mean value of  $37.3 \pm 4.9\%$ . Conversely, the highest LAP value was at T 3200 with an average of  $51.4 \pm 5.5\%$ . Upon further analysis, it was discovered that the inner regions of horizontal scans had the lowest LAP value at N 200, amounting to  $37.2 \pm 11.9\%$  whereas the highest LAP value within inner regions was recorded at T 400 with an average of  $76.4 \pm 8.5\%$ . Similarly, within the middle regions of horizontal scans, the lowest LAP value was noted at T 200, measuring  $8.3 \pm 8.8\%$  while the highest LAP value within middle regions was at N 2600 with a mean of  $43.0 \pm 8.2\%$ . With respect to the outer regions of horizontal scans, the lowest LAP value was documented at N 1700 with an average of  $45.7 \pm 5.8\%$  while the highest LAP value within outer regions was identified at T 3200, averaging  $64.6 \pm 7.4\%$ .

LAP measurements were compared between entire vertical and horizontal scans and all of the entire ROI, inner, middle and outer parts were significantly lower in the vertical group ( $p < 0.001$ ,  $p = 0.003$ ,  $p = 0.048$  and  $p < 0.001$ , respectively). (Table 2.)

**TCA**

Measurements of TCA were conducted on a sample of 100 eyes with scans executed both vertically and horizontally. In the vertical scans, observation of the total regions revealed that the mean value of TCA was lowest at I 3200 measuring  $23702 \pm 7269.4 \mu\text{m}^2$  while the highest value was observed at V 0, averaging  $30261.8 \pm 6869.5 \mu\text{m}^2$ . For the inner regions of vertical scans, the lowest TCA value occurred at I 3200, amounting to  $7801.5 \pm 2436.4 \mu\text{m}^2$ , and the highest value was recorded at I 100 with an average of  $9957.4 \pm 2262.2 \mu\text{m}^2$ . Similarly, within the middle regions of vertical scans, the lowest TCA value was noted at I 3200, measuring  $8211.8 \pm 2406.4 \mu\text{m}^2$  while the highest value was found at V 0 with a mean of  $10211.8 \pm 2271.6 \mu\text{m}^2$ . With respect to the outer regions of vertical scans, the lowest TCA value was documented at I 3200 with an average of  $7646.6 \pm 2489.8 \mu\text{m}^2$  while the highest value was identified at V 0, averaging  $9984.8 \pm 2319.2 \mu\text{m}^2$ . (Figure 2.)

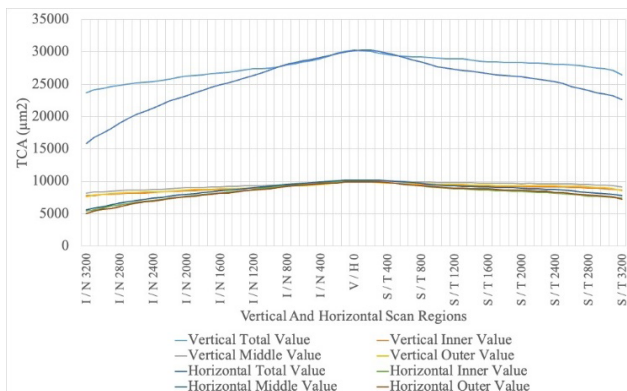


Figure 2. TCA Measurements in Vertical and Horizontal Scan Regions. TCA: Total Choroidal Area, I: Inferior, S: Superior, N: Nasal, T: Temporal, H: Horizontal, V: Vertical.

In the examination of total regions during horizontal scans, it was observed that the lowest TCA value was present at N 3200 with a mean value of  $15878.4 \pm 5328 \mu\text{m}^2$ . Conversely, the highest TCA value was found at 790

T 100 with an average of  $30288.2 \pm 7615.1 \mu\text{m}^2$ . For the inner regions within horizontal scans, the lowest TCA value was identified at N 3200, amounting to  $5423.5 \pm 1898.1 \mu\text{m}^2$ . Additionally, the highest TCA value within inner regions was recorded at H 0 with an average of  $10009.8 \pm 2549.3 \mu\text{m}^2$ . Similarly, within the middle regions of horizontal scans, the lowest TCA value was noted at N 3200, measuring  $5580.4 \pm 1824 \mu\text{m}^2$ . Correspondingly, the highest TCA value within middle regions was found at T 100 with a mean of  $10243.1 \pm 2519.5 \mu\text{m}^2$ . With respect to the outer regions of horizontal scans, the lowest TCA value was documented at N 3200 with an average of  $5021.6 \pm 1737.7 \mu\text{m}^2$ . In contrast, the highest TCA value within outer regions was identified at T 100, averaging  $9963.7 \pm 2536.3 \mu\text{m}^2$ . (Figure 2.)

Although there was no statistically significant difference in TRA between entire vertical and horizontal scan regions, in TCA all the measurements were found significantly higher in the vertical scans of entire ROI, inner, middle and outer parts ( $p = 0.010$ ,  $p = 0.013$ ,  $p = 0.012$  and  $p = 0.008$ , respectively). (Table 3.)

**LCA**

Measurements of the LCA were obtained through vertical and horizontal scans on a sample size of 100 eyes. In the vertical scans, the analysis of total regions revealed that the LCA value was at its minimum at I 3200 with a mean value of  $20984.2 \pm 7235.7 \mu\text{m}^2$  while the maximum LCA value was observed at V 0 with an average of  $26379.8 \pm 6956.5 \mu\text{m}^2$ . As for the inner regions of vertical scans, the LCA value was at its minimum at I 3200 amounting to  $7000.7 \pm 2415 \mu\text{m}^2$ , and the highest LCA value was recorded at I 100 with an average of  $8913.8 \pm 2345.9 \mu\text{m}^2$ . Similarly, the middle regions of vertical scans demonstrated the lowest LCA value at I 3200, measuring  $7120.7 \pm 2455.1 \mu\text{m}^2$  whereas the highest LCA value was found at S 300 with an average of  $8849.1 \pm 2392.3 \mu\text{m}^2$ . Regarding the outer regions of vertical scans, the lowest LCA value was documented at I 3200 with an average of  $6890.1 \pm 2507.9 \mu\text{m}^2$  whereas the highest LCA value within outer regions was identified at V 0 averaging  $8558.4 \pm 2491.8 \mu\text{m}^2$ .

During the examination of total regions in horizontal scans, the lowest LCA value was observed at N 3200 with a mean value of  $13199.8 \pm 5650.5 \mu\text{m}^2$ . Conversely, the highest LCA value was found at T 200 with an average of  $26555.2 \pm 7544.1 \mu\text{m}^2$ . In the inner regions of horizontal scans, the lowest LCA value occurred at N 3200 amounting to  $4513.6 \pm 2055.3 \mu\text{m}^2$ , and the highest LCA value within inner regions was recorded at H 0 with an average of  $8984.6 \pm 2602.8 \mu\text{m}^2$ . Similarly, within the middle regions of horizontal scans, the lowest LCA value was noted at N 3200 measuring  $4349.5 \pm 2220.7 \mu\text{m}^2$  while the highest LCA value within middle regions was found at H 0 with a mean of  $8800.8 \pm 2554.7 \mu\text{m}^2$ . The outer regions of horizontal scans documented the lowest LCA value at N 3200 with an average of  $4370.8 \pm 1828.7 \mu\text{m}^2$ . On the other hand, the highest LCA value within outer regions was identified at T 100, averaging  $8712.1 \pm 2810.5 \mu\text{m}^2$ .

LCA was measured and compared between entire

vertical and horizontal scans and LCA was found significantly higher in the vertical scans of entire ROI, inner, middle and outer parts ( $p = 0.014$ ,  $p = 0.014$ ,  $p = 0.008$  and  $p = 0.029$ , respectively). (Table 3.)

### SCA

The present study involved the implementation of SCA measurements in 100 eyes employing both vertical and horizontal scans. Upon analysis of the total regions in vertical scans, it was observed that the SCA value was lowest at S 1600 with a mean value of  $20117.6 \pm 1948.3 \mu\text{m}^2$  while the highest SCA value was documented at I 2700 exhibiting an average of  $29917.7 \pm 1502.3 \mu\text{m}^2$ . Upon further inspection of the inner regions of vertical scans, it was identified that the lowest SCA value was observed at S 1000 measuring  $2017.1 \pm 667.1 \mu\text{m}^2$  while the highest SCA value within inner regions was recorded at S 3000 with an average of  $29917.4 \pm 942.6 \mu\text{m}^2$ . Similarly, for the middle regions of vertical scans, it was determined that the lowest SCA value was documented at I 1400 amounting to  $2417.3 \pm 621.4 \mu\text{m}^2$  while the highest SCA value within middle regions was identified at S 1300 with a mean of  $29617.4 \pm 727.1 \mu\text{m}^2$ . With respect to the outer regions of vertical scans, the lowest SCA value was noted at I 3100 with an average of  $2017.4 \pm 626.4 \mu\text{m}^2$  while the highest SCA value within outer regions was identified at S 2200 exhibiting a mean of  $29817.9 \pm 1147.8 \mu\text{m}^2$ .

In the analysis of total regions during horizontal scans, the SCA value was found at its lowest at N 3200 with a mean value of  $2678.7 \pm 1374.4 \mu\text{m}^2$  while the highest SCA value was observed at T 2800 with an average of  $4252.8 \pm 2720.6 \mu\text{m}^2$ . Focusing on the inner regions of horizontal scans, the lowest SCA value was identified at T 1200 measuring  $740.5 \pm 494.5 \mu\text{m}^2$ , and the highest SCA value was documented at T 2600 with an average of  $1188.7 \pm 916.3 \mu\text{m}^2$ . Similarly, the middle regions of horizontal scans exhibited the lowest SCA value at N 1400, amounting to  $1001.8 \pm 785.5 \mu\text{m}^2$  while the highest SCA value within middle regions was found at T 2600 with an average of  $1668.5 \pm 1336.3 \mu\text{m}^2$ . In regards to the outer regions of horizontal scans, the lowest SCA value was observed at N 3100 with an average of  $645.7 \pm 681.8 \mu\text{m}^2$  while the highest SCA value within outer regions was identified at T 2800 with a mean of  $1533.7 \pm 1566.5 \mu\text{m}^2$ .

Comparison between entire vertical and horizontal scan measurements showed that SCA was not significantly difference in entire ROI, inner and middle parts ( $p = 0.471$ ,  $p = 0.815$ , and  $p = 0.521$ , respectively). (Table 3.)

### CVI

CVI measurements were made on 100 eyes for both vertical and horizontal scans. The lowest CVI value was observed at S 100 with a mean of  $66.4 \pm 8.9\%$  when assessing the total regions in vertical scans, and the highest CVI value was recorded at I 1200 with an average of  $71.7 \pm 8.4\%$ . The inner regions of vertical scans had the lowest CVI value at I 2500, measuring  $71.4 \pm 14.7\%$  while the highest CVI value within inner

regions was documented at I 1300 with an average of  $77.1 \pm 12.7\%$ . The lowest CVI value was noted at S 3200 for the middle regions of vertical scans amounting to  $61.3 \pm 22.3\%$  while the highest CVI value within middle regions was identified at I 500 with an average of  $71.3 \pm 16.6\%$ . Concerning the outer regions of vertical scans, the lowest CVI value was recorded at S 100 with an average of  $61.7 \pm 20.8\%$  while the highest CVI value within outer regions was noted at S 2300 with a mean of  $72.5 \pm 20.8\%$ .

When examining the total regions in horizontal scans, it was observed that the T 2800 exhibited the lowest CVI value with an average value of  $65.9 \pm 12\%$ . Conversely, the N 3100 displayed the highest CVI value with a mean value of  $73.6 \pm 10.7\%$ . Within the inner regions of horizontal scans, the lowest CVI value was recorded at N 200 measuring  $71.9 \pm 12.6\%$  while the highest CVI value within the same regions was identified at T 1000 with an average of  $78.3 \pm 12.5\%$ . With regards to the middle regions of horizontal scans, the lowest CVI value was noted at T 3200 with a value of  $59.4 \pm 20.9\%$ , and the highest CVI value within the said regions was documented at N 800 with an average of  $73.2 \pm 17.7\%$ . In terms of the outer regions of horizontal scans, the lowest CVI value was recorded at T 2800 with an average of  $63.9 \pm 27.8\%$  while the highest CVI value within the outer regions was noted at N 3100 with a mean of  $78.1 \pm 22.1\%$ .

CVI measurements compared between entire vertical and horizontal scans proved that CVI of the vertical scans of the entire ROI and outer parts were significantly lower than the horizontal ones ( $p = 0.019$  and  $p < 0.001$ , respectively). (Table 3.) Vertical measurement was significantly lower in the entire middle region ( $p = 0.025$ ). (Table 3.) There was no statistically significance between vertical and horizontal scans in the entire inner part ( $p = 0.678$ ). (Table 3.)

### SAP

Measurements utilizing Scanning Laser Polarimetry (SAP) were carried out on 100 eyes encompassing both vertical and horizontal scans. Upon evaluating the total regions of vertical scans, the SAP value was found lowest in I 1200, exhibiting a mean value of  $28.3 \pm 8.4\%$ . Conversely, the highest SAP value was observed in the total region identified as S 100 with an average value of  $33.6 \pm 8.9\%$ . In the inner regions of vertical scans, the SAP value was recorded as lowest at I 1300 measuring  $22.9 \pm 12.7\%$  while the highest SAP value was identified at I 2100 with an average of  $28.6 \pm 14.9\%$ . In the middle regions of vertical scans, the SAP value was noted as lowest at I 500 amounting to a value of  $28.7 \pm 16.6\%$  whereas the highest SAP value within middle regions was documented at S 3200 with an average of  $38.7 \pm 22.3\%$ . In reference to the outer regions of vertical scans, the SAP value was recorded as lowest at S 2300 exhibiting an average of  $27.5 \pm 20.8\%$  while the highest SAP value within outer regions was noted at S 100 with a mean of  $38.3 \pm 20.8\%$ .

When analyzing the comprehensive regions in horizontal scans, the SAP value was observed at its

lowest in N 3100 with an average value of  $26.4 \pm 10.7\%$ . Conversely, the highest SAP value was discovered in T 2800 with a mean value of  $34.1 \pm 12\%$ . Within the internal regions of horizontal scans, the SAP value was recorded at its minimum at T 1000 measuring  $21.7 \pm 12.5\%$  while the highest SAP value within internal regions was identified at N 200 with an average of  $28.1 \pm 12.6\%$ . In the midst of regions of horizontal scans, the SAP value was noted at its lowest at N 800 with a value of  $26.8 \pm 17.7\%$ , and the highest SAP value within the middle regions was documented at T 3200 with an average of  $40.6 \pm 20.9\%$ . Pertaining to the external regions of horizontal scans, the lowest SAP value was recorded at N 3100 with an average of  $21.9 \pm 22.1\%$  while the highest SAP value within external regions was noted at T 2800 with a mean of  $36.1 \pm 27.8\%$ .

SAP measurements between two scans, vertical and horizontal, were compared and SAP was significantly higher in the vertical scans than the horizontal scans in the entire ROI and outer parts ( $p = 0.019$  and  $p < 0.001$ , respectively). (Table 3.) However, it was found significantly lower in the entire middle region ( $p =$

**Table 1.** Table of General Overview

| Group                            | Value |
|----------------------------------|-------|
| Total Number of Subjects         | 50    |
| Total Number of Eyes             | 100   |
| Female to Male Ratio             | 1:1   |
| Total Number of Vertical Scans   | 100   |
| Total Number of Horizontal Scans | 100   |
| Total Number of OCT Scans        | 200   |

**Table 2.** Table of Entire Vertical and Horizontal Retinal Parameters.

| Parameter               | Group (n=100)      | Vertical Value $\bar{x} \pm \sigma$ | Horizontal Value $\bar{x} \pm \sigma$ |
|-------------------------|--------------------|-------------------------------------|---------------------------------------|
| TRA ( $\mu\text{m}^2$ ) | Entire ROI         | 2016004.9 $\pm$ 115693.8            | 2002003.9 $\pm$ 112419.9              |
|                         | Entire Inner Part  | 647759.3 $\pm$ 37952.9              | 643487.7 $\pm$ 37071.9                |
|                         | Entire Middle Part | 688058.8 $\pm$ 38574.9              | 682552.9 $\pm$ 37745.2                |
|                         | Entire Outer Part  | 674629.4 $\pm$ 39178.4              | 669556.4 $\pm$ 37727.4                |
| DRA ( $\mu\text{m}^2$ ) | Entire ROI         | 1089984.3 $\pm$ 79969.3             | 1058422.1 $\pm$ 86939.2               |
|                         | Entire Inner Part  | 280774.5 $\pm$ 19988.0              | 272571.6 $\pm$ 28985.4                |
|                         | Entire Middle Part | 459070.1 $\pm$ 34254.0              | 462889.2 $\pm$ 34000.5                |
|                         | Entire Outer Part  | 345291.7 $\pm$ 45715.0              | 319636.8 $\pm$ 43134.8                |
| LRA ( $\mu\text{m}^2$ ) | Entire ROI         | 926020.6 $\pm$ 50301.1              | 943581.9 $\pm$ 48685.2                |
|                         | Entire Inner Part  | 366984.8 $\pm$ 23432.3              | 370916.2 $\pm$ 23551.3                |
|                         | Entire Middle Part | 228988.7 $\pm$ 32443.5              | 219663.7 $\pm$ 28901.1                |
|                         | Entire Outer       | 329337.7 $\pm$ 27227.8              | 349919.6 $\pm$ 25438.9                |
| DAP (%)                 | Entire ROI         | 54.0 $\pm$ 1.5                      | 52.8 $\pm$ 2.0                        |
|                         | Entire Inner Part  | 43.3 $\pm$ 1.6                      | 42.3 $\pm$ 3.1                        |
|                         | Entire Middle Part | 66.8 $\pm$ 4.0                      | 67.8 $\pm$ 3.6                        |
|                         | Entire Outer Part  | 51.0 $\pm$ 4.7                      | 47.6 $\pm$ 4.5                        |
| LAP (%)                 | Entire ROI         | 46.0 $\pm$ 1.5                      | 47.2 $\pm$ 2.0                        |
|                         | Entire Inner Part  | 56.7 $\pm$ 1.6                      | 57.7 $\pm$ 3.1                        |
|                         | Entire Middle Part | 33.2 $\pm$ 4.0                      | 32.2 $\pm$ 3.6                        |
|                         | Entire Outer Part  | 49.0 $\pm$ 4.7                      | 52.4 $\pm$ 4.5                        |

%; Percentile;  $\bar{x}$ : Mean;  $\sigma$ : Standard Deviation; TRA: Total Retinal Area; DRA: Dark Retinal Area; LRA: Light Retinal Area; DAP: Dark Area Percent; LAP: Light Area Percent

0.025). (Table 3.) As in the CVI measurement, entire inner part measurements were not statistically different between vertical and horizontal parts. ( $p = 0.678$ ) (Table 3.)

**Table 3.** Table of Entire Vertical and Horizontal Choroidal Parameters.

| Parameter               | Group (n=100)      | Vertical Value $\bar{x} \pm \sigma$ | Horizontal Value $\bar{x} \pm \sigma$ |
|-------------------------|--------------------|-------------------------------------|---------------------------------------|
| TCA ( $\mu\text{m}^2$ ) | Entire ROI         | 1799591.2 $\pm$ 365971.8            | 1657121.6 $\pm$ 410068.5              |
|                         | Entire Inner Part  | 587126.5 $\pm$ 122421.1             | 541008.8 $\pm$ 137457.9               |
|                         | Entire Middle Part | 615141.2 $\pm$ 122360.8             | 568411.8 $\pm$ 137228.9               |
|                         | Entire Outer Part  | 592567.2 $\pm$ 121742.2             | 543947.1 $\pm$ 135597.5               |
| LCA ( $\mu\text{m}^2$ ) | Entire ROI         | 1569063.8 $\pm$ 360785.9            | 1434714.8 $\pm$ 404780.4              |
|                         | Entire Inner Part  | 524698.8 $\pm$ 121271.7             | 479497.8 $\pm$ 135504.9               |
|                         | Entire Middle Part | 530803.3 $\pm$ 121372.5             | 481400.1 $\pm$ 136964.7               |
|                         | Entire Outer Part  | 511224.5 $\pm$ 118786.5             | 472052.0 $\pm$ 132949.5               |
| SCA ( $\mu\text{m}^2$ ) | Entire ROI         | 230527.4 $\pm$ 81191.0              | 222406.8 $\pm$ 77903.1                |
|                         | Entire Inner Part  | 62427.6 $\pm$ 27504.9               | 61511.0 $\pm$ 27808.0                 |
|                         | Entire Middle Part | 84337.9 $\pm$ 29062.7               | 87011.7 $\pm$ 29720.7                 |
|                         | Entire Outer       | 81342.7 $\pm$ 27556.1               | 71895.0 $\pm$ 24605.1                 |
| CVI (%)                 | Entire ROI         | 69.2 $\pm$ 2.6                      | 70.1 $\pm$ 2.7                        |
|                         | Entire Inner Part  | 74.5 $\pm$ 4.6                      | 74.8 $\pm$ 5.0                        |
|                         | Entire Middle Part | 67.2 $\pm$ 3.9                      | 66.0 $\pm$ 4.1                        |
|                         | Entire Outer Part  | 66.6 $\pm$ 4.3                      | 70.3 $\pm$ 4.7                        |
| SAP (%)                 | Entire ROI         | 30.8 $\pm$ 2.6                      | 29.9 $\pm$ 2.7                        |
|                         | Entire Inner Part  | 25.5 $\pm$ 4.6                      | 25.2 $\pm$ 5.0                        |
|                         | Entire Middle Part | 32.8 $\pm$ 3.9                      | 34.0 $\pm$ 4.1                        |
|                         | Entire Outer Part  | 33.4 $\pm$ 4.3                      | 29.7 $\pm$ 4.7                        |

%; Percentile;  $\bar{x}$ : Mean;  $\sigma$ : Standard Deviation; TCA: Total Choroidal Area; LCA: Luminal Choroidal Area; SCA: Stromal Choroidal Area; CVI: Choroidal Vascularity Index; SAP: Stromal Area Percent

**Discussion**

TRA measurements in vertical scans showed that the lowest TRA value was recorded at V 0 and the highest at S 1200. This finding shows that the smallest area of 100  $\mu\text{m}$  interval is at the central retina, which corresponds to the foveola (1, 30). Accordingly, it is shown in the Figure 1. These findings are accurate and complementary to the retinal anatomical findings that are known before (1). Likewise, in its vertical analogue, the smallest area for TRA in horizontal scans was found at the central part which corresponds to the foveola mainly (1, 30). But interestingly the highest value shifted for 200  $\mu\text{m}$  from the vertical ones, which is N 1400 compared to the S 1200 which can be seen in the Figure 1.

Vertical and horizontal TRA results have been investigated and there was no statistically significant difference between entire ROI, entire inner part, entire middle part and entire outer part ( $p = 0.386$ ,  $p = 0.422$ ,  $p = 0.309$  and  $p = 0.352$  respectively). (Table 2.) Thus, alongside the retinal regions, total cross-sectional area of the retina is not different between horizontal and vertical scans. In the literature, there are studies conducted to investigate the horizontal and vertical scans in thickness measurement (31). The findings of the study demonstrated that there was a high level of concurrence at the group level, in the measurements

of thickness. Nevertheless, at the personal level, the level of concurrence was not that high (31).

DRA results should be interpreted with the TRA results, which is also lowest at the center. DRA results were interesting because all the equivalent parts of TRA was not different between vertical and horizontal scans. Thus, it can be said that dark area measurement through binarization of different topographical regions of the retina is used as a tissue distribution index to differentiate various conditions and diseases. It should be further investigated for the disease progression monitoring.

Entire LRA measurement comparison between vertical and horizontal scans showed a significant difference in the entire ROI, middle and outer parts, but not in the inner parts ( $p = 0.013$ ,  $p = 0.033$ ,  $p < 0.001$  and  $p = 0.238$  respectively.). (Table 2.) Combining the DRA results, light area measurement can be said to be an important marker at the middle parts whereas dark area measurement is a more prominent marker at the inner parts. They are both different and can be used as tissue distribution index at the outer parts of the retina. CVI and related parameters were measured and compared in many diseases (21-25, 32). These parameters and indexes mainly focused on the choroidal parameters. In the retinal part of this study, we mainly focused on the retinal parameters like TRA, DRA, LRA, DAP and LAP using image binarization methods which may be used for the diagnosis and follow up of different ophthalmological conditions. Alongside these measurements, DAP and LAP measurements are said to be good candidates for distinguishing different retinal topographic regions. The DRA, and LRA measurements exhibit a similarity to the TRA graph although there are some nuanced differences. Specifically, the DRA displays an augmented area in the inner central region while the LRA features an amplified area in the middle central region. Such disparities are believed to stem from the anatomical merge and vanishing of certain layers at the center of the fovea. TRA modifications are visually manifested in the aforementioned graphical alterations in Figure 1.

Findings of our study showed that between entire vertical and horizontal scan regions all TCA measurements were found significantly higher in the vertical scans of entire ROI, inner, middle and outer parts ( $p = 0.010$ ,  $p = 0.013$ ,  $p = 0.012$  and  $p = 0.008$ , respectively). (Table 3.) This situation was not observed at the TRA results. Thus, even retinal total areas are said to be evenly distributed, which is not the case for the choroidal part. This could be especially important for the nutritional supply of the retina and its topographical distribution alongside the eyeball. Many diseases affecting retina and choroid could be distinguished and even get prognosis using such markers, parameters and indexes. Choroidal thickness measurements alongside vertical and horizontal OCT scans were performed in the literature (33). Although in this study researchers did not investigate the choroidal area, they found that subfoveal choroidal thickness in healthy eyes in horizontal and vertical OCT scans were

not significantly different (33). And similar to the TRA results in our study, they found that the thickness of the subfoveal choroidal region had the greatest value compared to the other regions (33).

LCA findings of our study suggests that luminal part is considerably higher in the vertical scans through superior to inferior than horizontal scans through nasal to temporal which may suggest the more nutritional demand of the retina in that region. This finding may be important at various disease pathogenesis and have to be further investigated in the future studies in different conditions. SCA was significantly higher at the outer part of the choroid in vertical scans compared to the horizontal scans ( $p = 0.011$ ). (Table 3.) even though there seems to be a difference this finding should be interpreted with the TCA, which was also significantly higher in the entire vertical outer part ( $p = 0.008$ ).

The study findings suggest that CVI is lower in the entire ROI vertical scans, compared to the horizontal scans, but this is not the case for luminal area; although the area was found higher in the vertical scans, lumen per area was found higher in the horizontal scans. Thus, according to the results of nasal and temporal orientation, horizontal scans have a higher lumen per area, but have a lower total area compared to the vertical scans. Inner part of the choroid is more stable and is found relatively same at two different scan points, vertical and horizontal.

CVI has been investigated in many studies and many subject groups previously (21-25). Although there was no significant difference between choroidal thickness measurements, CVI, a parameter of choroid, was observed to decrease significantly in the AMD patients (26). Conversely CVI change was insignificant in the myopic choroidal neovascularization (CNV) patients who were treated with anti-vascular endothelial growth factor (VEGF) agents despite choroidal thickness change (34). Moreover, normal fellow eyes of the AMD patients found to have less CVI values, which demonstrates the signs of early changes could imply the CVI (35). Thus, CVI is investigated in a broad spectrum of diseases and the need for comparing the normalized data of different regions are increasing.

Our measurements of the choroidal region using CVI indicate that when centered to the fovea and with a 6500 mm range of the macula region, the vertical scans have a CVI of  $69.2 \pm 2.6$ , while the horizontal scans have a slightly higher value of  $70.1 \pm 2.7$ . However, these measurements increase to  $74.5 \pm 4.6$  and  $74.8 \pm 5.0$  in the inner one-third of the region, and decrease to  $66.6 \pm 4.3$  and  $70.3 \pm 4.7$  for the outer one-third of the region vertical and horizontal scans, respectively. (Table 3.) This difference between the inner and outer regions may be attributed to the anatomical nature of the choroid, which has choriocapillaris and SL in the inner regions, and HL and the choroidoscleral junction in the outer regions (4). The choriocapillaris is primarily responsible for nourishing the photoreceptor layer, and in our study, we found that the luminal area was increased. Interestingly, the CVI of the horizontal choroid increased in the outer regions compared to the vertical choroid, suggesting a greater need

for nourishment in the horizontal area. In our study we have found a slight difference between vertical and horizontal scan entire ROI CVI values with  $69.2 \pm 2.6$  and  $70.1 \pm 2.7$  respectively. This difference was significantly different at a p value of 0.019. CVI value change at this level could be interpreted as a slight change but especially considering the new emerging technologies regarding this topic, a close relative to image processing, artificial intelligence (AI) could help to distinguish between CVI change patterns in healthy and diseased eyes. Thus, this kind of precise data consisting topographical CVI changes could be utilized by AI, and might be considered a valuable tool for diagnosing and following up the diseases, especially with a rare presence and hard to diagnose.

Alongside CVI measurements, in this study, choroidal parameters and indexes like TCA, LCA, SCA and SAP and retinal parameters and indexes like TRA, DRA, LRA, DAP, LAP have been investigated. Both vertical and horizontal values have been investigated for 100  $\mu\text{m}$  interval 65 regions for retina and choroid. These 65 regions further investigated as inner, middle and outer parts as separate. Thus, normalized values, min and maximum values, and interactions between different scan regions have been investigated in this study.

The investigation of these parameters and calculations indexing healthy and diseased subjects can be improved in the future. An assessment of the normality limits for healthy eyes and the border for diseased eyes for every parameter can be carried out. Further research can include not only the macular region but also other anatomical regions such as the optic disk, peripheral retina, and vessels. Finally, the methodology may be applied to the recently introduced OCT modalities, and devices, even in the non-ophthalmological ones.

**Conflicts of Interest Statement:** Authors declare that there is no potential conflict of interest in this study.

**Financial Disclosure:** The authors declare that there is no financial support for this research

**Author Contributions:** Conception: O.İ., A.R.S., Design: O.İ., A.R.S., Supervision: O.İ., A.R.S., D.S., G.Ö.Ü. Materials: D.S., G.Ö.Ü., Data Collection: D.S., G.Ö.Ü., Analysis: O.İ., A.R.S., Literature Review: O.İ., Writer: O.İ., Critical Review: O.İ., A.R.S., D.S., G.Ö.Ü.

## References

- Gupta MP, Herzlich AA, Sauer T, Chan CC. Retinal Anatomy and Pathology. *Developments in ophthalmology*. 2016;55:7-17.
- Masland Richard H. The Neuronal Organization of the Retina. *Neuron*. 2012;76(2):266-80.
- Hildebrand GD, Fielder AR. Anatomy and Physiology of the Retina. In: Reynolds J, Oliitsky S, editors. *Pediatric Retina*. Berlin, Heidelberg: Springer Berlin Heidelberg; 2011. p. 39-65.
- Nickla DL, Wallman J. The multifunctional choroid. *Progress in retinal and eye research*. 2010;29(2):144-68.
- Ferrara D, Waheed NK, Duker JS. Investigating the choriocapillaris and choroidal vasculature with new optical coherence tomography technologies. *Progress in retinal and eye research*. 2016;52:130-55.
- Alm A, Nilsson SF. Uveoscleral outflow--a review. *Experimental eye research*. 2009;88(4):760-8.
- De Stefano ME, Mugnaini E. Fine structure of the choroidal coat of the avian eye. Lymphatic vessels. *Invest Ophthalmol Vis Sci*. 1997;38(6):1241-60.
- Bajwa A, Aman R, Reddy AK. A comprehensive review of diagnostic imaging technologies to evaluate the retina and the optic disk. *International ophthalmology*. 2015;35(5):733-55.
- Murthy RK, Haji S, Sambhav K, Grover S, Chalam KV. Clinical applications of spectral domain optical coherence tomography in retinal diseases. *Biomedical journal*. 2016;39(2):107-20.
- Boccara C, Dubois A. Optical Coherence Tomography. In: Goure J, editor. *Optics in Instruments: Applications in Biology and Medicine*. Wiley Online Books: John Wiley & Sons, Inc.; 2013.
- Huang D, Swanson EA, Lin CP, Schuman JS, Stinson WG, Chang W, et al. Optical coherence tomography. *Science (New York, NY)*. 1991;254(5035):1178-81.
- Hee MR, Puliafito CA, Wong C, Reichel E, Duker JS, Schuman JS, et al. Optical coherence tomography of central serous chorioretinopathy. *Am J Ophthalmol*. 1995;120(1):65-74.
- Schuman JS, Hee MR, Arya AV, Pedut-Kloizman T, Puliafito CA, Fujimoto JG, et al. Optical coherence tomography: a new tool for glaucoma diagnosis. *Current opinion in ophthalmology*. 1995;6(2):89-95.
- Hee MR, Baumal CR, Puliafito CA, Duker JS, Reichel E, Wilkins JR, et al. Optical coherence tomography of age-related macular degeneration and choroidal neovascularization. *Ophthalmology*. 1996;103(8):1260-70.
- Hee MR, Puliafito CA, Wong C, Duker JS, Reichel E, Rutledge B, et al. Quantitative assessment of macular edema with optical coherence tomography. *Archives of ophthalmology (Chicago, Ill : 1960)*. 1995;113(8):1019-29.
- Hee MR, Puliafito CA, Wong C, Duker JS, Reichel E, Schuman JS, et al. Optical coherence tomography of macular holes. *Ophthalmology*. 1995;102(5):748-56.
- Nassif NA, Cense B, Park BH, Pierce MC, Yun SH, Bouma BE, et al. In vivo high-resolution video-rate spectral-domain optical coherence tomography of the human retina and optic nerve. *Opt Express*. 2004;12(3):367-76.
- Sull AC, Vuong LN, Price LL, Srinivasan VJ, Gorczynska I, Fujimoto JG, et al. Comparison of spectral/Fourier domain optical coherence tomography instruments for assessment of normal macular thickness. *Retina*. 2010;30(2):235-45.
- Klein T, Wieser W, Reznicek L, Neubauer A, Kampik A, Huber R. Multi-MHz retinal OCT. *Biomed Opt Express*. 2013;4(10):1890-908.
- Margolis R, Spaide RF. A pilot study of enhanced depth imaging optical coherence tomography of the choroid in normal eyes. *Am J Ophthalmol*. 2009;147(5):811-5.
- Agrawal R, Gupta P, Tan KA, Cheung CM, Wong TY, Cheng CY. Choroidal vascularity index as a measure of vascular status of the choroid: Measurements in healthy eyes from a population-based study. *Scientific reports*. 2016;6:21090.
- Agrawal R, Chhablani J, Tan KA, Shah S, Sarvaiya C, Banker A. CHOROIDAL VASCULARITY INDEX IN CENTRAL SEROUS CHORIORETINOPATHY. *Retina*. 2016;36(9):1646-51.
- Agrawal R, Li LK, Nakhate V, Khandelwal N, Mahendradas P. Choroidal Vascularity Index in Vogt-Koyanagi-Harada Disease: An EDI-OCT Derived Tool for Monitoring Disease Progression. *Translational vision science & technology*. 2016;5(4):7.
- Agrawal R, Salman M, Tan KA, Karampelas M, Sim DA, Keane PA, et al. Choroidal Vascularity Index (CVI)--A Novel Optical Coherence Tomography Parameter for Monitoring Patients with Panuveitis? *PLoS One*. 2016;11(1):e0146344.
- Tan KA, Laude A, Yip V, Loo E, Wong EP, Agrawal R. Choroidal vascularity index - a novel optical coherence tomography parameter for disease monitoring in diabetes mellitus? *Acta ophthalmologica*. 2016;94(7):e612-e6.
- Wei X, Ting DSW, Ng WY, Khandelwal N, Agrawal R, Cheung

CMG. CHOROIDAL VASCULARITY INDEX: A Novel Optical Coherence Tomography Based Parameter in Patients With Exudative Age-Related Macular Degeneration. *Retina*. 2017;37(6):1120-5.

27.Schindelin J, Arganda-Carreras I, Frise E, Kaynig V, Longair M, Pietzsch T, et al. Fiji: an open-source platform for biological-image analysis. *Nature methods*. 2012;9(7):676-82.

28.Schneider CA, Rasband WS, Eliceiri KW. NIH Image to ImageJ: 25 years of image analysis. *Nature methods*. 2012;9:671.

29.Inam O. Calculation of choroidal vascularity index and tissue distribution indexes by digital processing of retinal and choroidal images obtained via optical coherence tomography [Doctorate Thesis]. Ankara: Hacettepe University Graduate School of Health Sciences; 2018.

30.Hoon M, Okawa H, Della Santina L, Wong RO. Functional architecture of the retina: development and disease. *Progress in retinal and eye research*. 2014;42:44-84.

31.Gonzalez Caldito N, Antony B, He Y, Lang A, Nguyen J, Rothman A, et al. Analysis of Agreement of Retinal-Layer Thickness Measures Derived from the Segmentation of Horizontal and Vertical Spectralis OCT Macular Scans. *Current Eye Research*. 2018;43(3):415-23.

32.Agarwal A, Agrawal R, Khandelwal N, Invernizzi A, Aggarwal K, Sharma A, et al. Choroidal Structural Changes in Tubercular Multifocal Serpiginoid Choroiditis. *Ocul Immunol Inflamm*. 2017:1-7.

33.Shin JW, Shin YU, Cho HY, Lee BR. Measurement of choroidal thickness in normal eyes using 3D OCT-1000 spectral domain optical coherence tomography. *Korean journal of ophthalmology : KJO*. 2012;26(4):255-9.

34.Ng WY, Ting DS, Agrawal R, Khandelwal N, Htoon HM, Lee SY, et al. Choroidal Structural Changes in Myopic Choroidal Neovascularization After Treatment With Antivascular Endothelial Growth Factor Over 1 Year. *Invest Ophthalmol Vis Sci*. 2016;57(11):4933-9.

35.Koh LHL, Agrawal R, Khandelwal N, Sai Charan L, Chhablani J. Choroidal vascular changes in age-related macular degeneration. *Acta ophthalmologica*. 2017;95(7):e597-e601.